Petroleum and Coal

Article **Open Access**

Rock-Physics-Model-Based Attributes and Seismic Inversion Controls for Reservoir Characterization: A Case Study of 'Rhoda' Field, Onshore Niger Delta Basin, Nigeria

Charles A. Illo, Mosto K. Onuoha*

University of Nigeria, Nsukka, Department of Geology, Nigeria

Received September 12, 2022; Accepted February 22, 2023

Abstract

Reservoir characterization entails mapping properties such as lithology, fluid type, porosity and permeability, to describe reservoir quality and identify areas for the location of new wells for optimum production. In this study, we test the reliability of rock-physics modelling and model-based post-stack seismic inversion for characterizing reservoir rocks located within the 'Rhoda' field, onshore Niger Delta Basin, Nigeria. The aim is to accurately discriminate lithology and estimate reservoir properties for accurate prediction of new prospective areas within the field of interest. Unlike some conventional inversion and geomodelling algorithms, which are probabilistic, model-based post-stack seismic inversion is favoured for its sensitivity in resolving thin-bed tuning for increased stratigraphic resolution and reservoir property prediction. More so, it gives satisfactory results, even with limited well control and fair to poor seismic quality, as will be shown in this study. On the basis of gamma-ray and resistivity log signatures, two reservoir sands, dubbed D6000 and D7000, were identified in the field of study. Along the eastern direction, well correlation revealed a significant net sand reduction. Within the reservoirs of interest, petrophysical parameters such as water saturation (S_w), porosity (∅), and shale volume (V_{sh}) were evaluated. With high ∅ and low S_w and V_{sh} values, these reservoirs were classified as good quality reservoirs. Crossplots of well-log properties such as density vs acoustic impedance, velocity ratio vs acoustic impedance, gamma-ray vs density, and gamma-ray vs acoustic impedance showed lithologies and pore fluids such as hydrocarbon sand, brine-sand, and shale. The model-based post-stack seismic inversion results revealed a lateral distribution of hydrocarbon and brine sands characterized by low and moderate acoustic impedance values, respectively. The low values of acoustic impedance slice and seismic horizon attributes (instantaneous phase and frequency) identified away from the drilled locations imply the presence of hydrocarbon-charged sands, which are potential prospects for future exploitation. This study therefore, shows the effectiveness of rock-physics-based modelling and model-based post-stack seismic inversion in the characterization of reservoir sands within the Niger Delta Basin and can be applied in other provinces around the world.

Keywords*: Niger Delta; Rock physics; Seismic inversion; Acoustic impedance; Reservoir characterization.*

1. Introduction

Reservoir characterization has gained prominence in the oil and gas industry due to the critical role it plays in reserve development by predicting reservoir properties such as lithology, porosity, permeability and fluid content at both local and regional scales [1-2]. An accurate model of these reservoir properties is required in order to drastically reduce the risks associated with hydrocarbon extraction from producing wells [2-3]. Rock-physics-based models and model-based inversion of 3D post-stack seismic data provides a platform for a thorough understanding of these reservoir attributes [2,4]. These methods have only recently gained popularity, and they are now commonly used for the estimation of reservoir properties in complex hydrocarbon reservoirs [[1-2,5]].

Rock-physics-based properties are reservoir properties that are obtained from well-log data for the purpose of improving subsurface predictions related to reservoir property distribution, which are otherwise confusing in standard well-log sections [2,6]. The relationship between these seismic rock-physics-based attributes and reservoir characterization provides a foundation for developing enhanced static and dynamic reservoir models, which provides information on changes in pore fluids, lithofacies, porosity, and permeability values [6-7]. These models have been employed successfully in prospecting for productive oil and gas fields as well as determining likely locations for exploratory and exploration wells [2,7].

On the other hand, 3D post-stack seismic inversion integrates reservoir properties to transform seismic reflection data into elastic parameters, allowing for the development of more accurate reservoir models [8-9]. It is a reliable tool for extracting lithofacies and petrophysical information from a sequential dataset [10-11]. The end result of seismic inversion leads to accurate characterization of reservoirs through the analysis of well-logs and seismic data for reservoir property prediction, which can then be used for delineating hydrocarbon targets [4, 9,12-13]. Unlike most conventional inversion approaches, model-based post-stack seismic inversion technique is deterministic, and is preferred due to its robustness and more direct hypothesis. It employs three main approaches; band-limited, sparse-spike, and model-based inversion. In model-based post-stack seismic inversion, the wavelet is convolved with a simple initial acoustic impedance to generate a synthetic response that is compared with the original seismic data. The model of the acoustic impedance is iteratively altered until the difference between the stacked seismic trace and the inverted trace is decreased to a threshold value. A model with a very small difference is accepted as a solution. The main seismic data itself acts as a guide for inversion and a wavelet can be simply derived straight from the seismic. Generally, the stacked seismic data is transformed into quantitative rock-physics parameters that are employed in reservoir characterization [12].

Using the ‘Rhoda’ field in onshore Niger Delta Basin as an example, this paper aims to demonstrate the usefulness of integrating rock-physics-based models and model-based post-stack seismic inversion in characterizing sub-surface reservoirs for the purpose of identifying new prospective areas that have not been previously drilled.

2. Basin description and geological setting

The Niger Delta Basin is situated within the Gulf of Guinea, which is located in the western part of Africa (Fig. 1a). It is currently the world's twelfth largest hydrocarbon province with a sub-aerial sediment cover of about 140,000 km^2 and a maximum thickness of 12 km [[14-15]. The delta, which is located on Africa's passive western edge, is thought to have a bent, wave- and tidal-shaped progradational pattern [16]. The Dahomey Basin forms the western boundary of the Niger Delta, while the Anambra Basin and the Gulf of Guinea form the northern and southern boundaries, respectively, with the Abakaliki Fold Belt and the Calabar Flank positioned at its eastern boundaries [14].

Although, the evolution of the basin is linked to the Cretaceous opening of the equatorial Atlantic [17], sediment progradation on the basin margin commenced in the late Eocene [18]. From the Eocene to the present, the delta has prograded south-west forming depobelts that define the delta's most intensively used portion at each stage of growth [14]. With an area extent of approximately 300,000 km^2 and a sediment volume of 500,000 km^3, these depobelts form one of the world's largest regressive deltas [19–21]. In response to the progradation of the Niger Delta sedimentary wedge, three major structural zones have been observed. They are (i) the extensional zone beneath the continental shelf; (ii) the transitional zone beneath the upper slope; and (iii) the compressional zone at the toe of the slope (Fig. 1b) [14].

After rifting seized, gravity controlled the deformational and depositional process and in late Eocene to early Pliocene, sediments of the petroliferous Niger Delta Basin were deposited. These sediments comprise up to 12 km thick of an upward coarsening regressive association of clastics that are strongly diachronous [21,22]. They include, from oldest to youngest; the Akata Formation, Agbada Formation and Benin Formation. The Akata Formation comprises thick, unstable and under-compacted shales that form a complex series of surfaces and depobelts. Overlying this formation are the denser paralic delta-front sands and shales of the Agbada Formation, which underlies the sands of the Benin Formation (Fig. 2). For any given depobelt, gravity tectonics were halted prior to the deposition of the Benin Formation and are expressed in complex features such as roll-over anticlines, shale diapirs, back-to-back faults, collapsed growth fault crests, and closely spaced, steeply dipping flank faults [14].

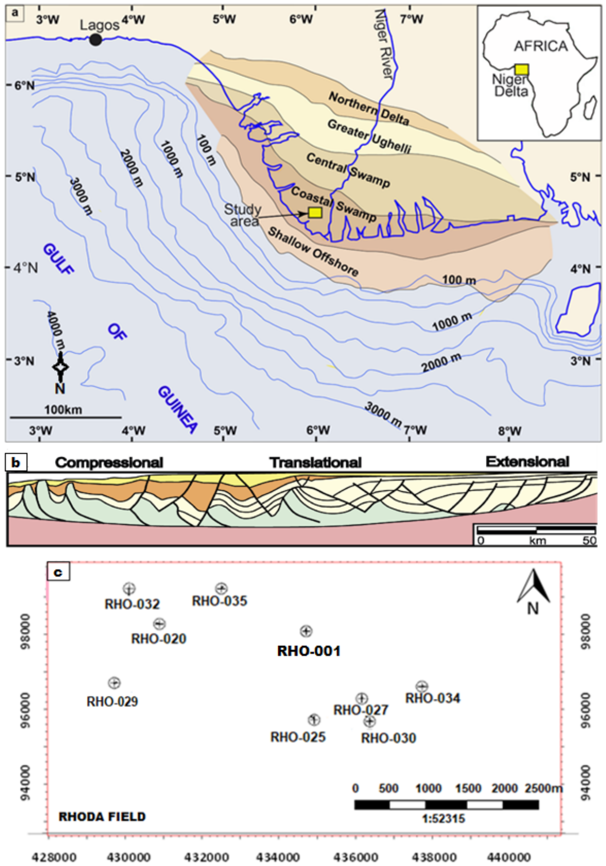

Fig. 1. (a) Map showing the location of the study area within the Niger Delta Basin (modified after Heiniö and Davies [40]). (b) The three structural divisions of the Niger delta (modified after [40]). (c) Centralized focus on Niger Delta Basin showing the studied RHODA hydrocarbon field and well distribution across the field.

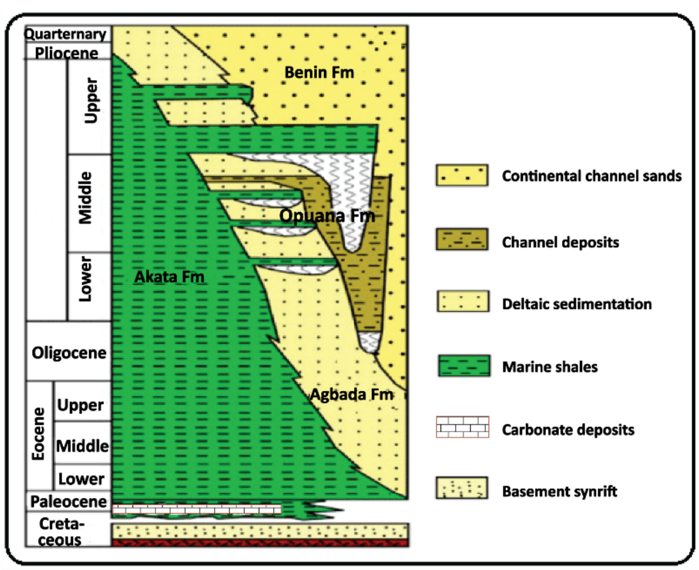

Fig. 2. Stratigraphy of the Niger Delta showing the lithologic units of the three formations (modified after Doust *et al.* [14]).

3. Conceptual framework

3.1. Rock physics models

To forecast reservoir properties from seismic and petrophysical data, it is necessary to model pore fluid impacts on elastic parameters such as P- and S-wave velocity, density, impedance, and velocity ratio [5]. The sensitivity of seismic responses to changes in reservoir parameters is investigated using rock physics modelling. The approach provides geophysicists with accurate knowledge for well-log data analysis and quality control, as well as evaluating seismic visibility of different fluid and lithology scenarios [6]. According to [23], rock physics analysis allows for easy understanding and interpretation when translating elastic parameters from well-log and seismic inversion data to reservoir parameters. The Gassmann's equation (Eqn. 1) is the most common technique used in simulating rock reaction resulting from different fluid saturations. The method establishes a relationship between saturated bulk modulus, porosity, bulk modulus of minerals in the rock matrix, and the bulk modulus of pore fluids [24].

$$K_{sat} = K_{dry} + \frac{\left(1-\frac{K_{dry}}{K_{ma}}\right)^2}{\left(\frac{\emptyset}{K_f}+\frac{1-\emptyset}{K_{ma}}+\frac{K_{dry}}{K_{ma}^2}\right)} \quad (1)$$

where K_{sat} is the saturated bulk modulus; K_{dry} is the bulk modulus of dry rock frame; K_{ma} is the bulk modulus of the rock matrix; K_f is the bulk modulus of pore fluids and φ is the porosity.

Gassmann's equation is based on a number of assumptions that must be considered prior to its application. These assumptions are (1) Rock (matrix and frame) must be macroscopically homogeneous, hence the wavelength must be larger than the pore and grain sizes; (2) All pores must be connected, which suggest that porosity and permeability must be large, with no isolated or weakly connected pores; (3) Pores must be saturated with a frictionless fluid; (4) The rock-fluid system must be closed; (5) There must be no interrelationship between fluid and matrix in a way that could cause a problem [25]. The saturated bulk modulus, Ksat, can be predicted using these assumptions. Thereafter, the value of Ksat is used to estimate the P- and S-wave velocities as shown in Eqns. 1 and 2 [25]:

$$V_p = \sqrt{\frac{K_{sat}+\mu}{\rho b}} \quad (2)$$

$$V_s = \sqrt{\frac{\mu}{\rho b}} \quad (3)$$

where K_{sat} is the saturated bulk modulus; V_p is the P-wave velocity; V_s is the S-wave velocity; ρb is the bulk density; and μ is the shear modulus (modulus of rigidity).

3.2. Post-stack seismic inversion

The process for converting seismic reflection data to quantifiable reservoir properties is known as seismic inversion. Post-stack seismic inversion technique is based on certain criteria that are mathematically inclined. The two basic concepts that underpin post-stack seismic inversion approaches in this work are (i) the seismic trace s(t) can be defined by the convolution of the reflectivity coefficient series r(t) with a band-limited wavelet w(t) and the addition of a random noise n(t) (Eqn. 4) and (ii) the earth could be characterized domestically by utilizing a stack of smooth and uniform beds having continuous physical attributes:

$$S(t) = r(t) + n(t) \quad (4)$$

Aimed at negligible normal incidence, r(t) is proportional to the difference in the acoustic impedance (AI) of overlying strata as shown below [26]:

$$r_j = \frac{AI_{j+1} - AI_j}{AI_{j+1} + AI_j} \quad (5)$$

where r_j is the reflection coefficient at the jth interface of a set of N superposed layers, and AI = ρv, where ρ and v are correspondingly the density and P-wave velocity.

From this perspective and supposing that several reflectors are removed from seismic surveys, the AI value of a piece surface may be approximated using a recursive calculation based on an understanding of the AI value of the layer beyond [26]:

$$AI_{j+1} = AI_j\left(\frac{1+r_j}{1-r_j}\right) \quad (6)$$

This can then be simplified to obtain the AI value of every M layer by multiplying by:

$$\mathrm{AI_M} = \mathrm{AI_1}\prod_{\mathrm{j=2}}^{\mathrm{M}}\left(\frac{1+\mathrm{r_j}}{1-\mathrm{r_j}}\right) \quad (7)$$

In order to obtain a linear approximation, we compute the natural logarithm of both sides of Eqn. 7:

$$\ln\,(AI_M) = \ln\,(AI_1) + \sum_{i=2}^{M} 2\left[r_i + \frac{r_i^3}{3} + \frac{r_i^5}{5} + \cdots\right] \quad (8)$$

This allows us to drop the high-order variables which lead to Eqn. 9 as given below:

$$AI_M = AI_1\,exp\left(2\,\sum_{j=2}^{M} r_j\right) \quad (9)$$

In recursive inversion, Eqn. 9 is a useful formula for converting seismic reflectivity to impedance. The top layer's recognized acoustic impedance is AI_1, while the Mth layer's is AI_M. The jth layer's reflection coefficient is rj. For the vast majority of realistic scenarios where $r_j \leq |0.3|$, this estimate is known to be accurate [4,26,27].

4. Dataset and methods

4.1. Dataset

The dataset used in this study includes well-logs and 3D post-stack seismic data. In the 'Rhoda' field, a total of nine (9) wells, named RHO-001, RHO-020, RHO-025, RHO-027, RHO-029, RHO-030, RHO-032, RHO-034, and RHO-035 (see Fig. 1c), were drilled, with total vertical depths (TVD) of 11,900 ft, 11, 850 ft, 11,980 ft, 12,000 ft, 12,100 ft, 12,300 ft, 12,400 ft, 12,100 ft, and 12,300 ft respectively. Only RHO-001 and RHO-030 penetrated reservoirs of interest and were considered in the present study. Petrophysical logs including gamma-ray, resistivity, density and sonic, and reservoir markers, were available in the studied wells. The seismic data consists of 779 inlines and 449 crosslines, characterized by horizontal spacing of 25 x 25 meters and vertical seismic resolution of 20 m.

4.2. Methods

In order to achieve the aim of characterizing reservoirs in 'Rhoda' field, onshore Niger Delta, we carried out (i) well-log conditioning, correlation and petrophysical analysis, (ii) well-to-seismic tie and horizon picking, (iii) model-based post-stack seismic inversion, (iv) rock physics analysis and (v) surface attributes analysis.

4.2.1. Well-log conditioning, correlation and petrophysical analysis

Well-log data conditioning (DC) was employed to compensate for spikes in the data that may have occurred due to noise and logging effects. Log filtering and checkshot correction were the quality control procedures used on the log data. To compensate for anomalies in the sonic derived P-wave log signatures, the sonic logs were corrected using checkshot. Afterwards, log filtering was performed using six (6) as the operator length. The selected operator length is appropriate for removing irregular high-frequency spikes thereby improving the signal-to-noise ratio. Well correlation was employed to identify and relate similar patterns of rocks/reservoirs across wells.

Petrophysical modelling was used to determine the reservoir characteristics of the zones of interest, in particular, the D6000 and D7000 reservoirs, which were identified by their low gamma and high resistivity log signatures. Reservoir properties such as porosity, water saturation, and shale volume were determined within the reservoir's defined boundaries. The reservoir porosity was measured using the equation below [5]:

$$\emptyset = \frac{\rho_{ma} - \rho_b}{\rho_{ma} - \rho_f} \quad (10)$$

where ρ_b is the formation's bulk density; ρ_{ma} is the rock matrix density; and ρ_f the fluid density that fills the pore spaces.

The relationship defined by [28] was employed in the estimation of water saturation level as shown in Eqn. 11 below:

$$S_w^n = \frac{a}{\emptyset^m} X \frac{R_w}{R_t} \tag{11}$$

where *a* describes the cementation factor; m signifies the cementation exponent; R_w represents the resistivity of the formation water, and n indicate the saturation exponent.

The volume of shale (V_{sh}) is a petrophysical parameter that defines the quantity of shales that is present within a particular reservoir interval. Shaliness is crucial in determining the lithology make-up of a reservoir interval and is thus useful for characterizing its porosity and water saturation levels. In this study, V_{sh} was determined by adopting the well-known Larinov equation (Eqn. 12), which is used to estimate the degree of shaliness of Tertiary sediments [29].

$$V_{sh} = 0.083 X \left[2^{(3.7 X IGR)} - 1\right] \tag{12}$$

Generally, sediments are classified as clean sand, shaly-sand, or shale in accordance with the V_{sh} cut-offs estimates obtained. The cut-offs are categorized as follows:

1. V_{sh} < 10% indicates a clean sand [30],
2. V_{sh} estimates between 10 – 35% indicates shaly-sand, and
3. V_{sh}> 35% indicates a shale zone [31].

where IGR represents the gamma-ray index and expressed by [5] as:

$$IGR = \frac{GR_{log} - GR_{min}}{GR_{max} - GR_{min}} \tag{13}$$

where GR_{log} is the GR value of the formation measured from log; GR_{min} is the GR minimum value of clean sand; and GR_{max} is the shale beds' GR maximum value.

4.2.2. Well-to-seismic tie and horizon mapping

In this study, the first stage of seismic inversion was to correlate the well-log and seismic data, then calibrate them by generating a synthetic seismogram using the RHO-001 well in the 'Rhoda' field. Acoustic impedance was calculated based on the convolution of sonic and density logs at the well location in relation to the target reservoirs. Subsequently, the calculated impedance was converted to reflectivity. A synthetic seismogram was then generated by convolving the reflectivity derived from the acoustic impedance with an acceptable wavelet. The best wavelet for this analysis was found by repeatedly extracting various wavelets and selecting the one that had the best association between well synthetic (blue traces) and composite trace (red traces).

Horizon mapping was carried out on the 3D seismic data using a standard auto-tracking approach, which aided the delineation of several horizons [32-33]. These horizons are surfaces that separate different rock layers in depositional environments characterized by different reflection properties [33]. Seismic to well integration was essential in tying these horizons (reflection events) to their corresponding depths in the petrophysical logs.

4.2.3. Model-based post-stack seismic inversion

Model-based post-stack seismic inversion is based on the convolutional theory which suggests that the seismic trace may be formed by convolving a wavelet with the earth's reflectivity and adding noise [4]. To do so, the wavelet phase and frequency are estimated using reflection coefficient series from wells within the boundaries of seismic survey. The success of post-stack seismic inversion relies majorly on accurate estimation of the wavelet.

This seismic inversion approach is based on the delineation of reservoir properties such as lithology and fluid content. Firstly, a synthetic seismogram was generated to create a connection between the well logs and seismic data after which a low-frequency model was generated by interpolating well log acoustic impedance along the delineated horizons. This background model is critical, in that when compared to other conventional alternative inversion processes used to invert seismic sections, it yields a higher efficiency especially when well logs are only employed [1].

4.2.4. Rock-physics-based analysis

Integrated analysis of attributes such as density, P-Impedance, and Vp/Vs_ratio aided the accurate estimation of reservoir porosity, lithology, and associated fluid contents. Analysis of these rock physics parameters produces a more reliable result of reservoir properties compared to the conventional presentation and visual assessment of generated crossplots of associated well log properties [34].

Since the well-log data provided for this study lacked S-wave logging data, the well-known Castagna relationship [35] for sand and shale beds was used to generate an S-wave from the well logs (Eqn. 14). This linear relation, which is extensively applied for generating S-wave velocity logs all over the world is expressed below:

$$V_s = a \, X \, V_p + b \tag{14}$$

where V_s is the S-wave velocity; V_p is the P-wave velocity; a = 0.8619; and b = -3845.14.

Acoustic impedance (P-Impedance) was estimated from a linear equation involving density (ρ) and P-wave velocity is given [4] as shown in Eqn. 15 below:

$$P - Impedance = V_p \, X \, \rho \tag{15}$$

Velocity ratio (Vp/Vs_ratio) was obtained from the non-linear relationship of P-Impedance and S-Impedance (Shear Impedance). The relation is expressed in Eqn. 16 as given by [33]:

$$Velocity\ ratio = \frac{AI}{SI} = \frac{\rho V_p}{\rho V_s} = \frac{V_p}{V_s} \tag{16}$$

4.2.5. Surface attributes analysis

Geophysical signatures observed in a seismic data which wholly or in part aid hydrocarbon recognition, lithological classification, or geologic understanding is referred to as seismic attributes [36]. In addition to 3D model-based post-stack seismic inversion, we conducted 3D seismic attributes analysis to identify probable hydrocarbon-saturated zones. This was accomplished by a thorough examination of seismic characteristics and horizon slices [37].

Using the Hampson Russell software, we generated instantaneous phase, instantaneous frequency, and acoustic impedance slice from the inverted 3D seismic section. The instantaneous phase, a sensitive parameter, measures the phase components of wave propagation and is used for detecting lateral sand continuity. The instantaneous frequency responds to both wave propagation effects and depositional characteristics and gives a measure of bed thickness and hydrocarbon presence [38]. The acoustic impedance slice highlights the association of seismic traces by allocating green to yellow colours to areas that correspond to low acoustic impedance, red to areas of moderate acoustic impedance, and blue to purple colours to areas of high acoustic impedance [39]. Potential zones such as unconsolidated sands and hydrocarbon-charged compartments were identified using these surface attributes.

5. Results and interpretation

5.1. Well-logs and petrophysical analysis

Well log correlation reveals the existence of two reservoirs; D6000 and D7000 (Fig. 3). As illustrated in Figs 4, 5, and 6, the reservoir parameters of the 'Rhoda' field were derived from the well-log signatures of RHO-001 and RHO-030. The log signatures describe the defined reservoir sand zones assigned as D6000 and D7000, which have been circled in dotted blue eclipse. The relationships between the obtained petrophysical properties were used to map these zones.

The intervals with low gamma-ray and high resistivity log values were interpreted as hydrocarbon-saturated sands based on the integrated analysis. Away from the reservoir units, however, intervals described by high gamma-ray and low resistivity values correspond to shale lithology (Figs 4, 5, and 6). Facies range from shale deposits at the reservoir's base to sand deposition at the reservoir's tip. The Niger Delta Formation lithologic series, where the research area is situated, is represented by sand and shale lithological divisions (see Fig. 2).

Low P-Impedance and Vp/Vs Ratio values associated with delineated reservoir zones correspond to hydrocarbon-saturated sand, while moderate to high values outside the reservoir intervals reveal background shales (Figs. 4, 5 and 6, Track 4). The low water saturation values (<10%) associated with reservoir zones correspond to high presence of hydrocarbon fluid compared to zones showing high water saturation values outside the reservoir units, which are interpreted as brine fluids (Figs. 4, 5 and 6; track 3). High porosity values (>30%) are noticed within the reservoir units compared to low porosity values (<30%) observed outside the reservoir units (Figs. 4, 5 and 6; Track 1). In comparison to low porosity values interpreted as non-reservoir shaly compartments, the high porosity values associated with the delineated reservoirs units correspond to good-quality reservoirs.

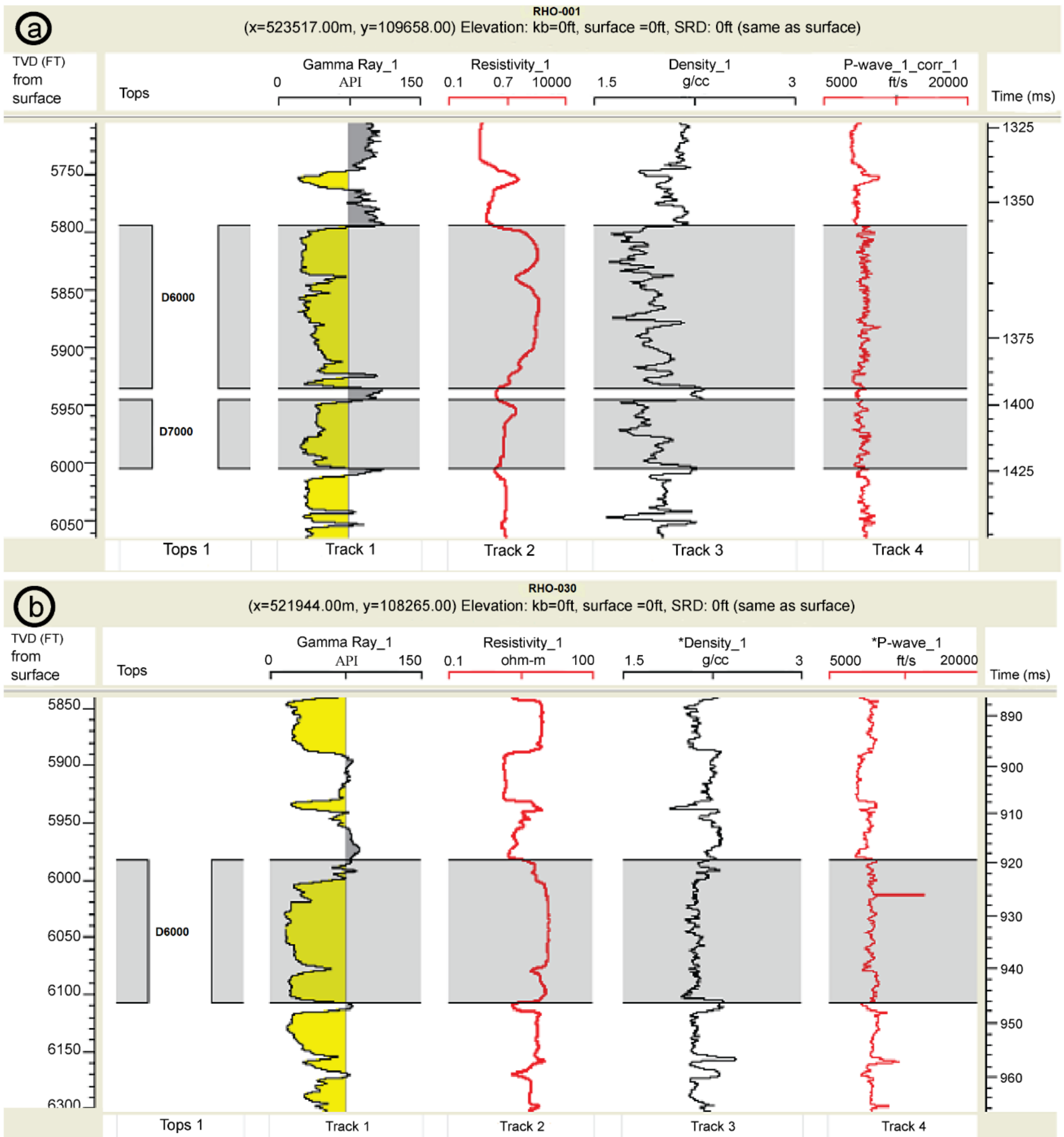

Fig. 3. Well logs section display showing delineated D6000 and D7000 reservoirs, and lithology relationship across logs in RHO-001 and RHO-030 wells. Within the defined reservoir units, the sands show low gamma ray values while shales indicate higher gamma ray signatures outside the reservoir units.

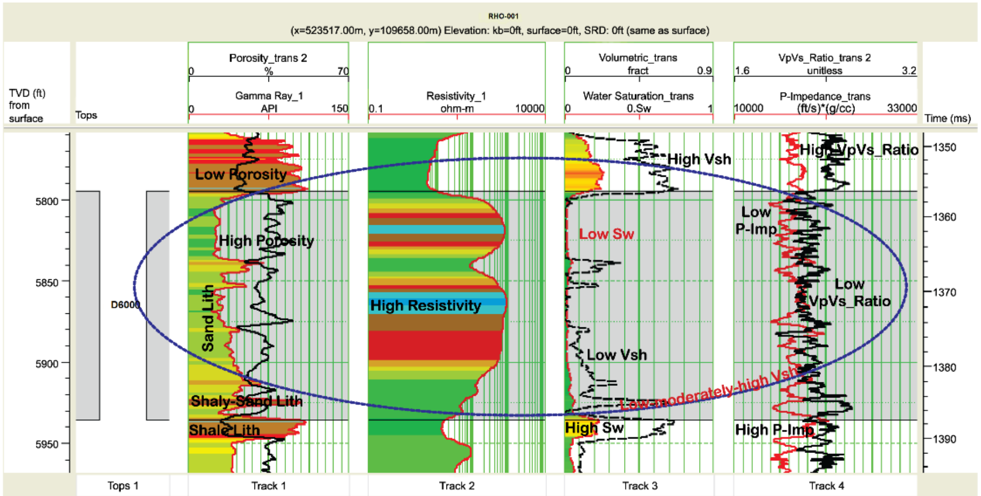

Fig. 4. RHO-001 well showing the D6000 reservoir and its estimated reservoir parameters.

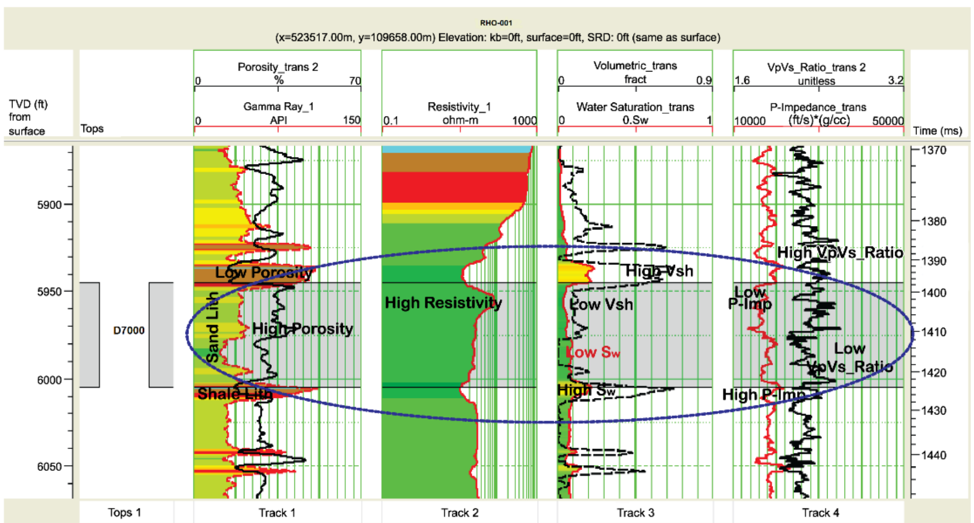

Fig. 5. RHO-001 well showing the D7000 reservoir and its estimated reservoir parameters.

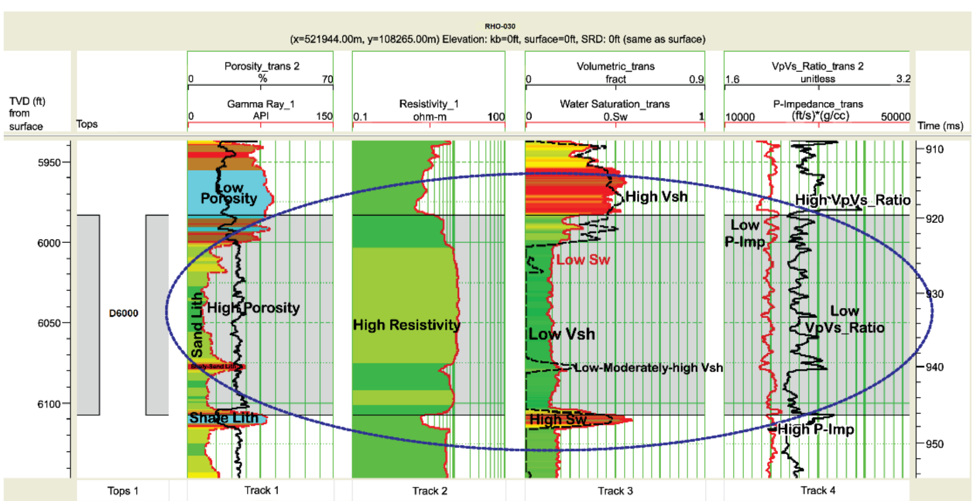

Fig. 6. RHO-030 well showing the D6000 reservoir and its estimated reservoir parameters.

The volume of shale (Vsh) was found to be low (<25%) within the reservoir intervals and high (>45%) away from the reservoir units (Figs. 4, 5 and 6; Track 3). The low Vsh values associated with the reservoir zones correspond to high presence of unconsolidated sand deposits which makes up the reservoir units. The observed intervals inside the reservoir units showing low to moderately-high Vsh values were interpreted as shaly-sand lithologies while the zones outside the reservoir units corresponds to high Vsh values indicating shale rock accumulations (Figs. 4 and 6; Track 3).

Correlation of wells RHO-001 and RHO-030 shows differences in thicknesses down dip across the wells for the D6000 designated sand reservoir (Fig. 7). In comparison to the RHO-030 well, the D6000 reservoir sand in RHO-001 is thicker. This suggests that D6000 sand was deposited much nearer to RHO-001 well. The reservoirs range from 5795 – 5935 and 5945 – 6005 ft in RHO-001 well for D6000 and D7000, respectively, while in RHO-001 well, the reservoir ranges from 5985 – 6105 ft for D6000. These limits of values assign reservoir thicknesses of 140 and 120 ft across RHO-001 and RHO-030 wells for D6000 reservoir respectively, and 60 ft for D7000 reservoir within RHO-001 well.

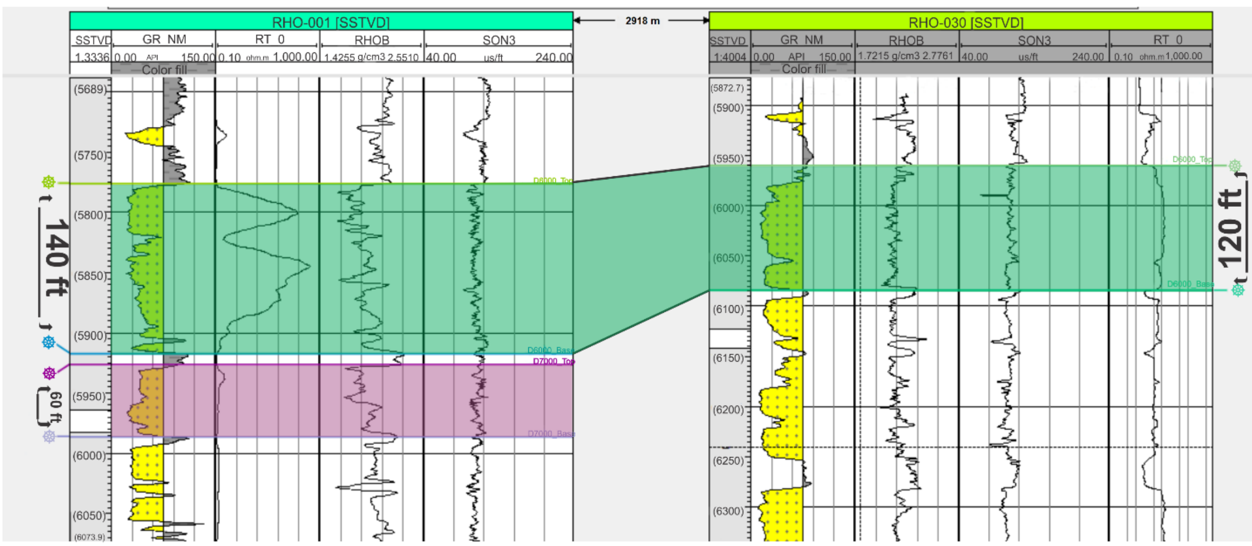

Fig. 7. Well log correlation of RHO-001 and RHO-030 wells showing variation in reservoir thickness.

5.2. 3D model-based post-stack seismic inversion analysis

The initial low-frequency acoustic impedance model is displayed in Fig. 8a. A relatively acceptable correlation was obtained between the original synthetic trace and the inverted result (see Fig. 9). The model-based acoustic impedance seismic section generated through post-stack seismic inversion was characterized by low, moderate, and high acoustic impedance attribute (AIA) values (Fig. 8b). The AIA key displayed by the right-hand side of the inverted volume reveal values that range from 15908 – 26868 ft/s * (g/cc). The colours associated with the AIA key, indicating changes in reservoir properties like lithology and pore fluid, are represented within the entire volume in various compartments. The zone indicated towards the upper part (1200 – 1460 ms) of the inverted volume where the horizons (HZA_TOP, HZA_BASE, HZB_TOP AND HZB_BASE) were delineated shows a dominance of green and yellow colours indicating low AIA values. However, the lower part (1500 – 1800 ms), which shows red and blue colouration represents zones with moderate to high AIA values (Fig. 8b). The examined reservoir units are defined within the seismic intervals that ranges between 1355 – 1390 ms (5795 – 5935 ft) for reservoir unit between HZA_TOP and HZA_BASE, and 1397 – 1423 ms (5945 – 6005 ft) for the second reservoir interval that falls between HZB_TOP and HZB_BASE (Fig. 8b).

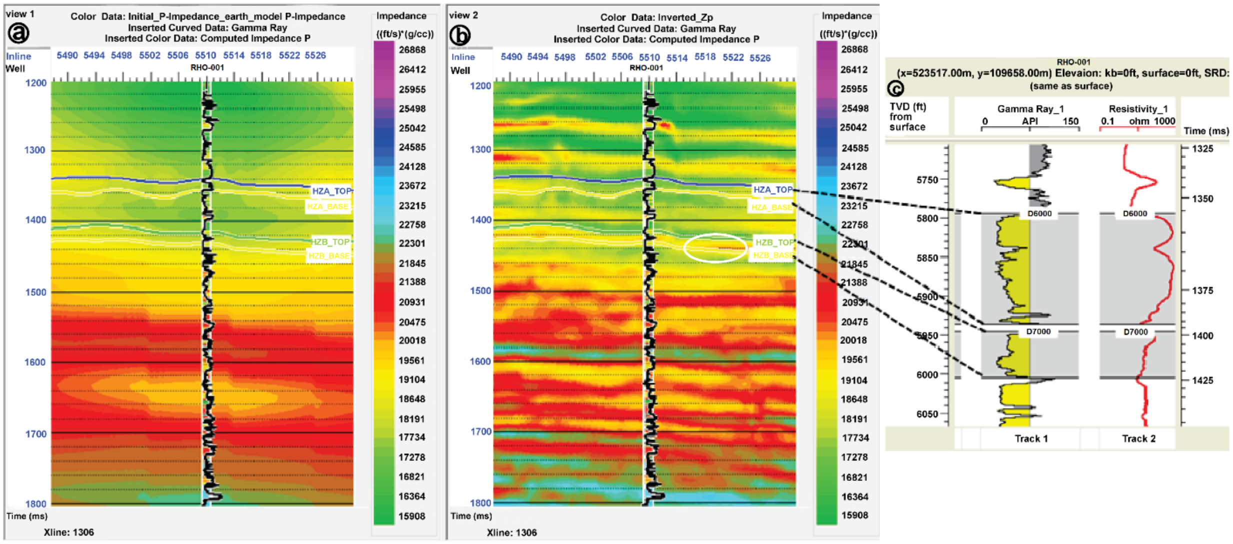

Fig. 8. (a) Initial low-frequency impedance model utilized for the generation of inverted acoustic impedance volume of the 'Rhoda' field (b) The inverted acoustic impedance seismic volume showing the D6000 (1355 – 1390 ms) and D7000 (1397 – 1423) reservoir units, and the position of the RHO-001(c) RHO-001 well section showing the reservoirs and their correlation to HZA_Top and HZB_Top seismic intervals.

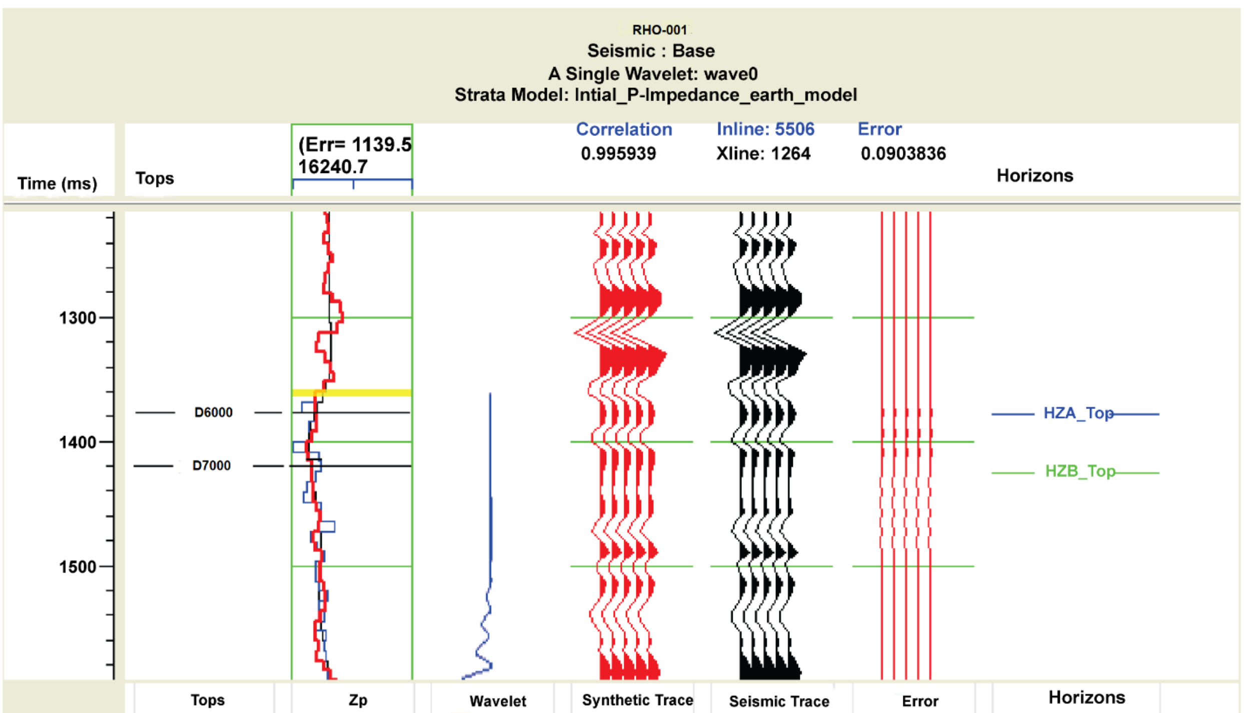

Fig. 9. Model-based seismic inversion analysis showing a relatively acceptable correlation between the original log (red) and inverted result (black) for RHO-001 well.

The proximal zones of the two reservoir units display more of green and yellow colours indicating low AIA zones, while the distal part reveals more variation of yellow and red colours suggesting zones with changes in AIA values (Fig. 8b; white eclipse). The RHO-001 well with an inserted gamma-ray log was defined within the inverted seismic volume, which penetrated the reservoir units at their corresponding intervals (Fig.8b). Fig 8c displays the gamma-ray and resistivity log signatures of the defined reservoir seismic intervals. The sealing shales at the top and bottom of the two reservoir intervals (Fig. 8c) are revealed much better when compared to the inverted section (Fig. 8b).

The reservoir zone associated with green and yellow colours, with low AIA values (PAK <20,018) was interpreted as hydrocarbon-saturated sand [4,9] (Fig. 8b). The distal portion of the reservoir unit associated with moderate AIA values (20,050<AIA< 22,301), which is more evident in the seismic interval between HZB_TOP and HZB_BASE corresponds to brine-saturated sands indicated by the white eclipse in Fig. 11b [4]. The zones with blue colour outside the reservoir intervals, at the southern part of the inverted section, associated with high AIA values (> 22,301) (Fig. 8b) was interpreted as shale accumulations [4].

5.3. 3D rock physics-based model analysis

Well-log attributes such as gamma-ray, density, P-impedance and Vp/Vs_ratio within the D6000 reservoir of RHO-001 well were used to generate crossplot models of density versus P-impedance, Vp/Vs_ratio versus P-impedance, gamma-ray versus density, and gamma-ray versus P-impedance (Fig. 10). Within the crossplot domains, clusters indicating variations in rock properties were represented by different colours. These colours were assigned from changes in values of the attribute key at the right-hand side of the models (Fig. 10).

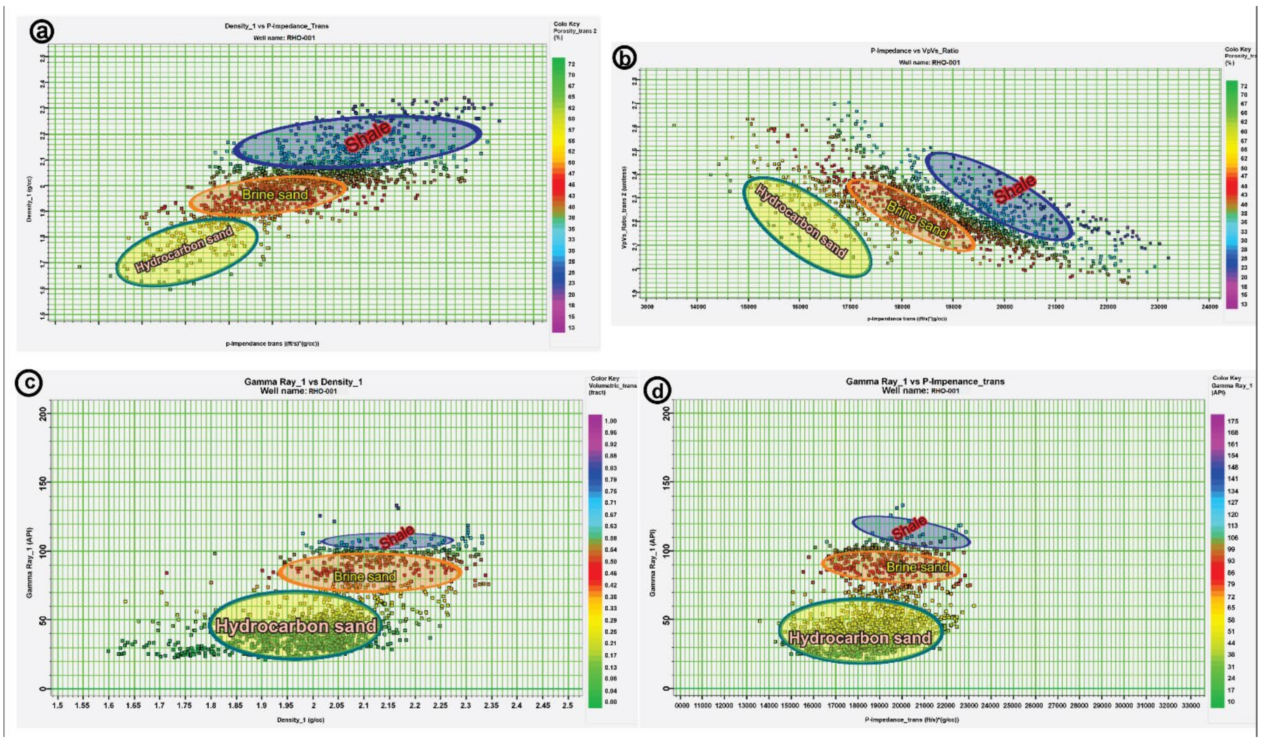

Fig. 10. Rock physics models from RHO-001 well (a) Density vs P-Impedance (b) Vp/Vs_ratio vs P-Impedance. (c) Gamma-ray vs Density (d) Gamma-ray vs P-Impedance. Hydrocarbon sands (yellow eclipse), brine sands (red eclipse) and shale (blue eclipse) display low, moderate and high values of crossplotted well-log attributes, respectively.

A well-derived density against P-impedance crossplot colour coded with porosity is shown in Fig. 10a. The result shows an increase in porosity with decreasing density and P-impedance attributes within the yellow eclipse, which corresponds to hydrocarbon-saturated sand. Clusters above the hydrocarbon-saturated sand represented by red and blue eclipses, and showing moderate to high values of density and P-impedance, were interpreted as brine-filled sands and shale lithologies respectively.

Figs 10b, c and d show crossplot of Vp/Vs_ratio versus P-impedance, gamma-ray versus density, and gamma-ray versus P-impedance colour coded with porosity, V_{sh} and gamma-ray respectively. The cross-plots show an increase in porosity with decreasing Vp/Vs_ratio and P-

Impedance, decrease in V_{sh} with decreasing gamma-ray and density, and a decrease in gamma-ray values with a corresponding decrease in P-impedance within the yellow eclipses indicating hydrocarbon-saturated sands (Figs 10b, c and d). Clusters above the delineated hydrocarbon-saturated zone, indicated by red eclipses with moderate Vp/Vs_ratio and P-impedance values, gamma-ray and density values, and gamma-ray and P-Impedance, suggests brine-filled sands. Similarly, clusters above the brine-filled sands that are represented in blue eclipses with moderately-high Vp/Vs_ratio and P-Impedance values, gamma-ray and density values, and gamma-ray and P-impedance, are interpreted as background shales (Figs 10b, c and d).

5.4. 3D horizon attributes and lithological classification

HZA_TOP, HZA_BASE, HZB_TOP, and HZB_BASE, the boundaries of our reservoirs of interest, were mapped on the seismic section after well to seismic tie (Fig. 11). Detailed analysis of seismic attributes and horizon slice focused on HZB_TOP since HZA_TOP indicates a comparatively lower acoustic impedance suggesting more hydrocarbon presence when compared to HZB_TOP. This enabled the identification and characterization of probable hydrocarbon-bearing sands situated away from well locations within the delineated horizon. Instantaneous phase extraction at the top of continuous low impedance seismic package, confirmed the occurrence of NE and SW trend zones, characterized by low (red – yellow colours) and high (white – blue) instantaneous phase values respectively (Fig. 12). The zones enclosed in green eclipses that are laterally continuous from the hydrocarbon charged sands at drilled locations, and are associated with low instantaneous phase values, were interpreted as sand lithologies. On the other hand, portions indicated in blue colours with high instantaneous phase values are indicative of shales [38].

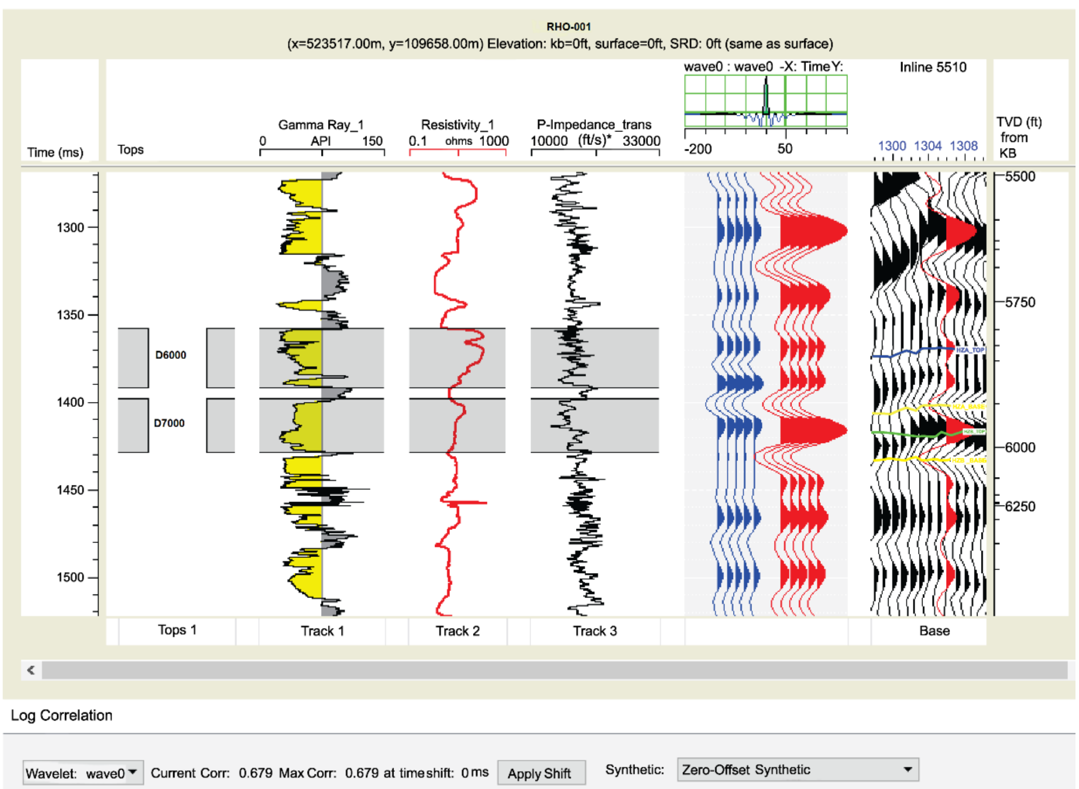

Fig. 11. A sample of well to seismic tie based on the generation of synthetic seismogram for D6000 and D7000 reservoirs in RHO-001 well. The correlation value between well synthetic (blue traces) and composite trace (red traces) from seismic data is about 0.68.

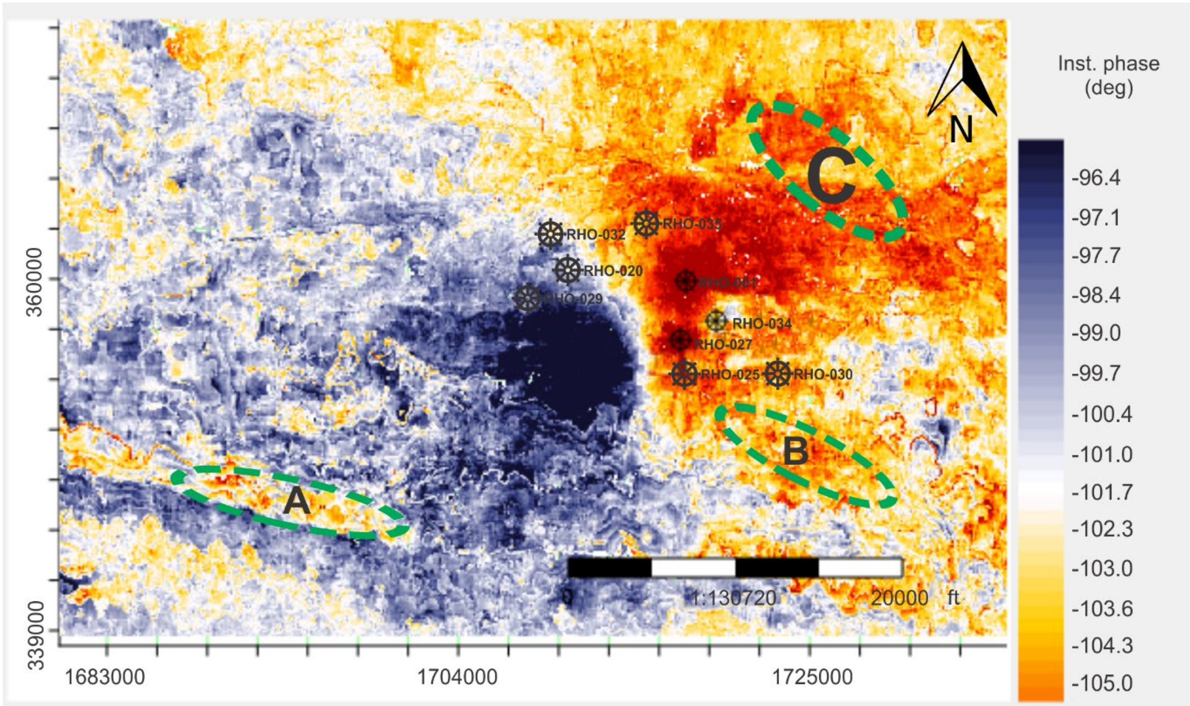

Fig. 12. Instantaneous phase map at HZB_Top showing hydrocarbon-charged sand-rich sediments across the field. Circled zones (A, B and C) are new prospective areas for well drilling.

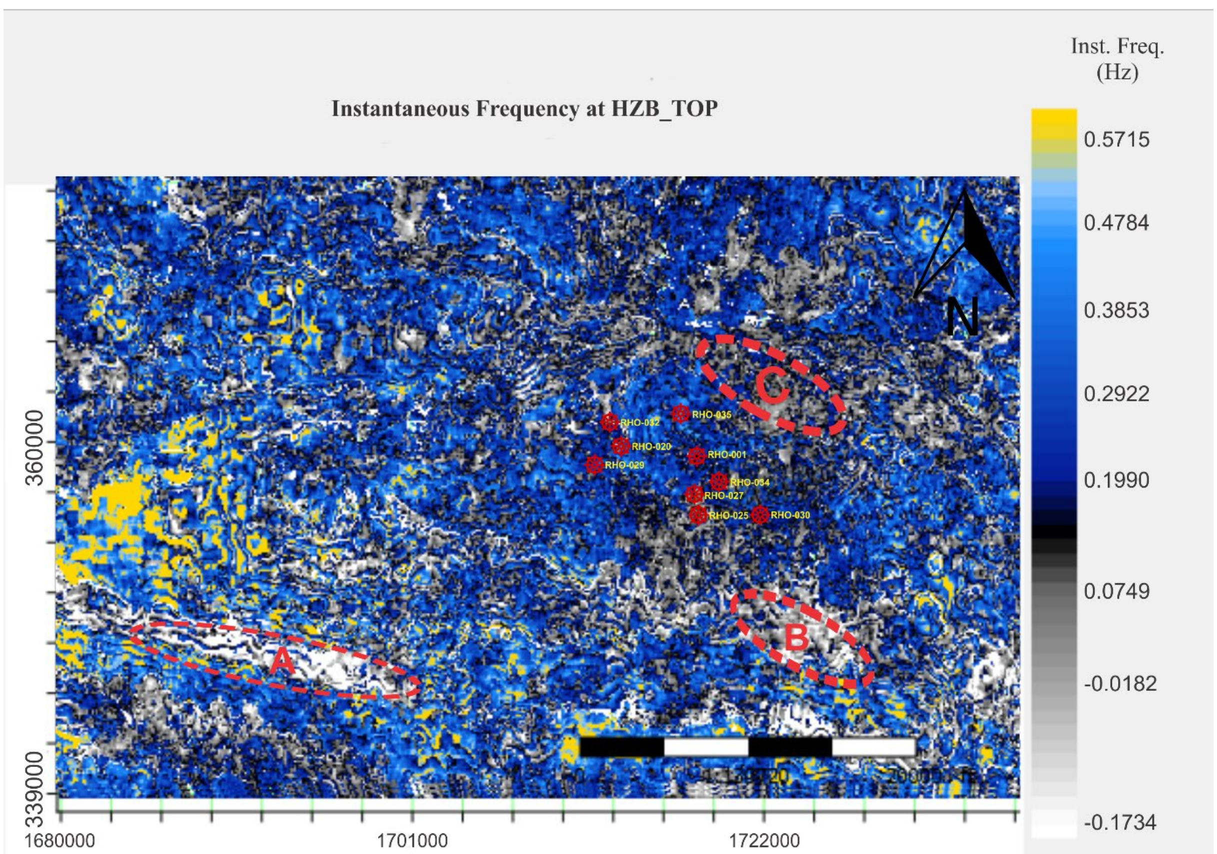

Fig. 13. Instantaneous frequency map at HZB_Top showing hydrocarbon-charged sand-rich sediments across the field. Zones A, B, and C are favourable areas for well drilling.

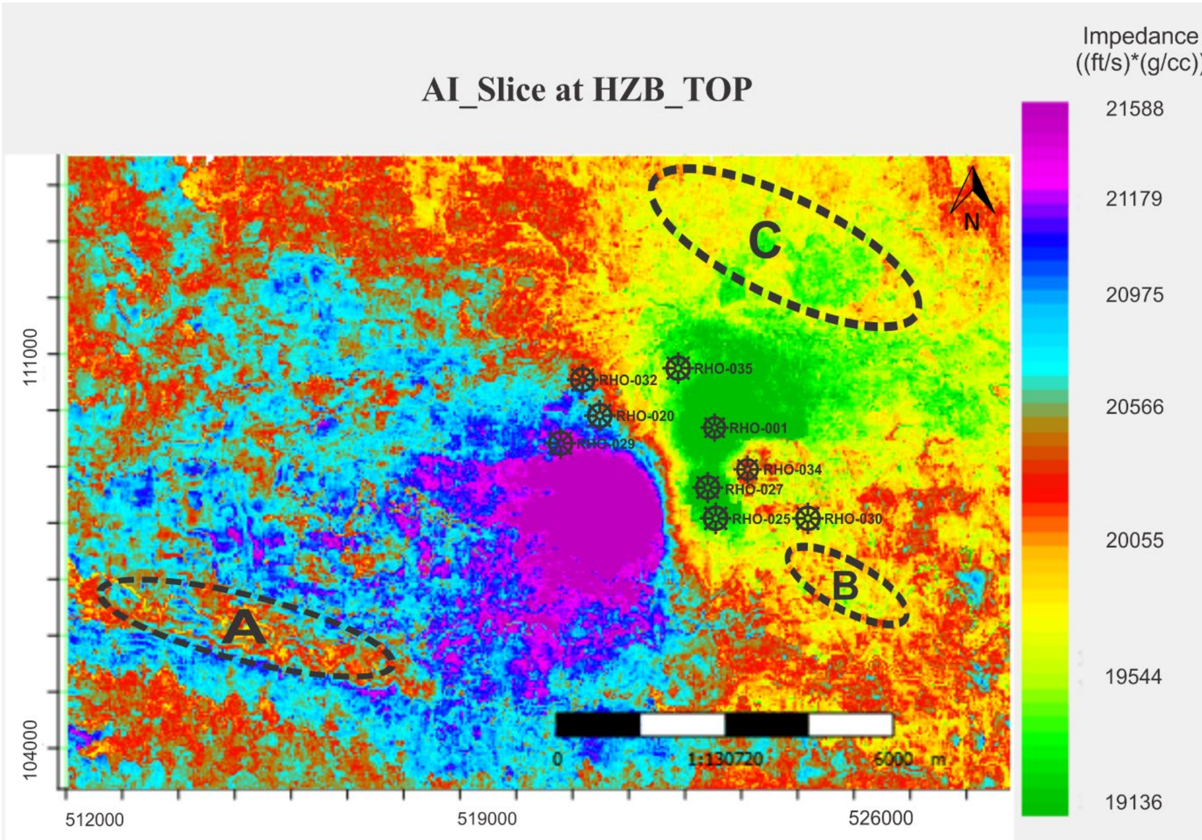

Fig. 14 Acoustic impedance slice at HZB_Top showing hydrocarbon-charged sand-prone lithologies across the field and recommended zones (A, B and C) for new well drilling.

The instantaneous frequency is characterized by low and high values in different compartments (Fig. 13). The zones marked with red eclipses away from well locations, and associated with low instantaneous frequency anomaly indicate hydrocarbon-saturated-sands whereas areas characterized by blue and yellow colourations with moderate to high instantaneous frequency values represents shale deposits [38] as seen in Fig. 13.

The acoustic impedance slice reveals the occurrence of NE and SW compartments that are characterized by low (green – yellow), moderate (red) and high (blue – purple colours) acoustic impedance values (Fig. 14). The zones away from drilled locations denoted with black eclipses and associated with low acoustic impedance values are interpreted as zones of unconsolidated hydrocarbon-charged sands (Fig. 14). However, zones represented with red colours and associated with moderate acoustic impedance values, indicate brine-filled sands. Compartments that are characterized by high acoustic impedance values were inferred as shale zones [39].

6. Discussion

6.1. Petrophysical evaluation and reservoir quality assessment

The well logs and petrophysical parameters from this study suggest that lithology discrimination between sand and shale is probable. The P-impedance logs and the high porosity sandstone facies showed a clear association. The hydrocarbon-saturated sand zones in the studied formation often correspond to the lower P-impedance values from rock physics model study. In the well-attribute crossplot results, the shale facies are distinguished by strong P-impedance values. As a result, we used the rock physics model as a stand-alone exercise for well-log data interpretation and quality control, as well as to determine seismic detectability of various fluid and lithology scenarios. Furthermore, near the base, the reservoir intervals have low to moderately high Vsh values (Figs. 5 and 7; Track 3). This could be linked to shale intrusion that was reported in the arcuate Niger Delta Formation [5]. When comparing the thickness of the D6000 reservoir between the wells, the RHO-001 well showed a higher thickness of about 20 ft and a higher porosity than the RHO-030 well. As a result, the area around the RHO-001 well possesses more hydrocarbon storage space and better pore connectivity for fluid flow. This study has shown good correlation between rock-physics models and facies/fluid characterization, which has been previously shown by previous authors that attempted reservoir delineation and quality assessment using well-logs and petrophysical properties [5].

6.2. Seismic inversion and Reservoir lateral distribution

The horizon cross sections (HZA_Top and HZB_Top) that cut across the RHO-001 well show a good indication of the lateral lithological distribution within the specified reservoir zones. The fluid saturation of the distributed sands is given more attention (See Fig. 8b). The low AIA values confirm our initial result, which suggests that the sand lithologies are mainly saturated with hydrocarbon fluids as shown by these horizon cross sections. Also, as the inverted segment progresses, the AIA values appear to increase. The reason for this increase is probably due to the substitution of hydrocarbon fluids with brine fluids during production. Therefore, the fluid distribution in the Niger Delta Basin is primarily controlled by reservoir depletion (Fig. 8b). This study, therefore, has provided an explanation for the major cause of fluid saturation lateral distribution in the Niger Delta Basin, which is not contained in previous works that attempted a modelling of reservoir fluid distribution in some hydrocarbon fields in the Niger Delta region [12-13].

6.3. Rock physics and reservoir properties variation

Within the examined reservoir unit, rock physics models formed from crossplots of related well-log attributes generated from the RHO-001 well reveal three distinct lithological zones; hydrocarbon sand, brine sand, and shale (Fig. 10). In comparison with the red (brine-filled sands) and blue (background shales) eclipses, the yellow eclipses (hydrocarbon-saturated sands) have slightly different clustering points. As a result, it may be possible to identify hydrocarbon-bearing sands in the ‘Rhoda’ field, which could be used in constraining seismic inversion results. Owing to the robust sensitivity of elastic parameters to various lithologies and pore fluids, hydrocarbon-saturated sands can be clearly distinguished from brine-filled sands and shales. In line with the work of [2], which used pre-stack simultaneous inversion in forecasting lithofacies and fluid content in the ‘Goliat’ field, and the work of [7] which attempted to classify reservoir properties distribution in various fields using rock physics templates, this work was able to distinguish lithology and pore fluid.

6.4. Lithologic distribution and prospect evaluation

Figs. 12, 13 and 14 are detailed examples of lithology distribution across the area. The generally low values of acoustic impedance slice and horizon attributes suggest that the wells drilled across the field targeted compartments made up of sand-rich sediments. However, from these maps produced from the horizon interpretation, other sand-rich sediments were deposited in the northeast and southwest zones of the field, which have not been drilled. The low values acoustic impedance slice, instantaneous phase and instantaneous frequency extracted over the defined seismic interval within the vicinity of the sand-prone lithologies showed the occurrence of bright spots amplitudes that conform to structures indicated by Eclipses A, B and C shown in Figs. 12, 13 and 14. These are good indicators of possible hydrocarbon accumulation. In line with the study of [7-8], this study has successfully delineated new prospects of unconsolidated sands across the ‘Rhoda’ field, which should be considered for infill well drilling for high economic recovery.

7. Conclusion

Rock-physics based models, model-based post-stack seismic inversion and surface attributes has enabled the characterization of D6000 and D7000 reservoirs of the ‘Rhoda’ field, onshore Niger Delta. Rock-physics based models based on well-log attributes crossplot analysis revealed the existence of two lithologies, which are sand and shale, and two fluid types; hydrocarbon and brine. Petrophysical evaluation shows reservoirs that are of good to very good quality. In the research area, reservoir correlations along the strike and dip demonstrate a net sand reduction basinward and eastwards. Model-based acoustic impedance inversion adjusted to well control revealed better geological understanding of the reservoir lateral distribution from identified horizons. Horizon attributes such as instantaneous phase, instantaneous frequency and acoustic impedance slice indicated three zones of unconsolidated sands and probable hydrocarbon accumulation. In conclusion, this study has shown the effectiveness of rock-physics based approach, model-based post-stack seismic inversion, horizon and petrophysical attribute analysis in reservoir characterization in the Niger Delta Basin, which enabled a better understanding of reservoir quality and distribution as well as reservoir heterogeneities within the basin, thus reducing uncertainties associated with prospects identification and well developments.

Acknowledgement

The authors are thankful to the Department of Petroleum Resources (DPR) and Shell Petroleum Development Company (SPDC), Nigeria, for providing the needed data for the preparation of this study. The first author acknowledges with thanks, the technical support provided by Mr. Timi Tralagba.

Declarations

Conflict of Interest:*The authors have no conflict of interests to declare that are relevant to the content of this article.*

Funding: *No funding was received for conducting this study.*

Author contribution: *CAI participated in data curation, formal analysis, data interpretation and manuscript drafting, while* MKO conceptualized and validated the project.

References

[1] Kadkhodaie-Ilkhchi R, Moussavi-Harami R, Rezaee R, Nabi-Bidhendi M, Kadkhodaie-Ilkhchi A. Seismic inversion and attributes analysis for porosity evaluation of the tight gas sandstones of the Whicher Range field in the Perth Basin, Western Australia. J. Nat. Gas Sci. and Eng. 2014; 21:1073-83.

[2] Yenwongfai HD, Mondol NH, Faleide JI, Lecomte I. Prestack simultaneous inversion to predict lithology and pore fluid in the Realgrunnen Subgroup of the Goliat Field, southwestern Barents Sea. Interpretation. 2017; 5(2):75-96. https://doi.org/10.3997/2214-4609.201600964.

[3] Yoong AA, Lubis LA, Ghosh DP. Application of simultaneous inversion method to predict the lithology and fluid distribution in "X" Field, Malay Basin. In: IOP Conference Series: Earth and Environ. Sci. 2016; 38(1):012007. https://doi.10.1088/1755-1315/38/1/012007.

[4] Maurya SP, Sarkar P. Comparison of post stack seismic inversion methods: a case study from Blackfoot Field, Canada. Int. J. Scient. Eng. Res. 2016; 7(8):1091-101.

[5] Akpan AS, Okeke FN, Obiora DN, Ibuot JC. Fluid substitution modelling and derived rock attribute-based discriminations of hydrocarbon and lithology: a case study of arcuate Niger Delta Depobelt, Nigeria. SN Appl. Sci. 2020; 2(12):1-8. https://doi.org/10.1007/s42452-020-03855-z.

[6] Avseth P. Explorational rock physics: the link between geological processes and geophysical observables. In: Petroleum Geoscience (pp. 455-488). Springer, Berlin, Heidelberg. 2015. https://doi.org/10.1007/978-3-642-02332-3_18.

[7] Azeem T, Chun WY, Khalid P, Ehsan MI, Rehman F, Naseem AA. Sweetness analysis of Lower Goru sandstone intervals of the Cretaceous age, Sawan gas field, Pakistan. Epis. J. Int. Geosci. 2018; 41:235-247.

[8] Farfour M, Yoon WJ, Kim J. Seismic attributes and acoustic impedance inversion in interpretation of complex hydrocarbon reservoirs. J. Appl. Geophy. 2015; 114:68-80.

[9] Karim SU, Islam MS, Hossain MM, Islam MA. Seismic reservoir characterization using model based post-stack seismic inversion: in case of fenchuganj gas field, Bangladesh. J Japan Petro Institute. 2016; 59(6):283-292.

[10] Pendrel J. Seismic inversion—The best tool for reservoir characterization. CSEG Recorder. 2001; 26(1):18-24.

[11] Abdel-Fattah MI, Pigott JD, El-Sadek MS. Integrated seismic attributes and stochastic inversion for reservoir characterization: Insights from Wadi field (NE Abu-Gharadig Basin, Egypt). J Afri. Earth Sci. 2020; 161:103661.
[12] Austin OE, Onyekuru Smauel I, Ebuka AO, Abdulrazzaq ZT. Application of model-based inversion technique in a field in the coastal swamp depobelt, Niger Delta. International Journal of Advanced Geosciences. 2018; 6(1):122-6.
[13] Eze S, Orji OM, Nnorom SL, Ubogun K. Model Based Inversion of Acoustic Impedance from Seismic Trace for Lithofacies Differentiation: an Application in Xy Field Offshore Niger Delta. J Appl Sci & Environ Mgt. 2019; 23(9):1677-1684. https://dx.doi.org/10.4314/jasem.v23i9.12.
[14] Doust H, Omatsola E. Niger Delta. In: Edwards JD, Santogrossi PA (eds) Divergent/passive Margin Basins, AAPG Memoir 48, Tulsa, Oklahoma, 1990; pp. 239-248.
[15] Tuttle WL, Brownfield EM, Charpentier RR. The Niger Delta Petroleum System. Chapter A: Tertiary Niger Delta (Akata-Agbada) Petroleum System, Niger Delta Province, Nigeria, Cameroon and Equatorial Guinea, Africa. US Geolgical Survey, Open File Report. US Geological Survey, Open File Report. 1999:99-50.
[16] Anyiam OA, Eradiri JN, Mode AW, Okeugo CG, Okwara IC, Ibemesi PO. Sequence stratigraphic analysis and reservoir quality assessment of an onshore field, Central Swamp Depobelt, Niger Delta Basin, Nigeria. Arab. J. Geosci. 2019; 12(24):1-9. https://doi.org/10.1007/s12517-019-4954-3.
[17] Evamy BD, Haremboure J, Kamerling P, Knaap WA, Molloy FA, Rowlands PH. Hydrocarbon habitat of Tertiary Niger delta. AAPG Bulletin. 1978; 62(1):1-39.
[18] Reijers TJ, Petters SW, Nwajide CS. The Niger delta basin. In: Sedimentary basins of the world. Elsevier. 1997; 3: 151-172.
[19] Hospers J. Gravity field and structure of the Niger delta, Nigeria, West Africa. Geological Society of America Bulletin. 1965; 76(4):407-22.
[20] Kaplan A, Norton IO, Lusser CU. Tectonic map of the world: scale 1:10,000,000. American Association of Petroleum Geologists, Tulsa, 1985.
[21] Kulke H. Regional Geology of the world, part 2: Africa, America, Australia. Antarctica: Berlin Gebrulder borntraeger, Kulke Ed. 1995; 143-172.
[22] Burke KC, Dessauvagie TF, Whiteman AJ. Geological history of the Benue valley and adjacent areas. African Geology. 1972; 1(8):7-2.
[23] Avseth P, Veggeland T. Seismic screening of rock stiffness and fluid softening using rock-physics attributes. Interpretation 2015; 3(4):SAE85-93. https://doi.10.1190/INT-2015-0054.1.
[25] Mavko G, Bandyopadhyay K. Approximate fluid substitution for vertical velocities in weakly anisotropic VTI rocks. Geophysics. 2009; 74(1):D1-6. [24] Gassmann F. Elastic waves through a packing of spheres. Geophysics. 1951; 16(4): 673-685.
[26] Leite EP, Vidal AC. 3D porosity prediction from seismic inversion and neural networks. Computers & Geosciences. 2011; 37(8):1174-1180. https://doi.org/10.1016/j.cageo.2010.08.001.
[27] Berteussen KA, Ursin B. Approximate computation of the acoustic impedance from seismic data. Geophysics. 1983; 48(10):1351-1358.
[28] Archie GE. Classification of carbonate reservoir rocks and petrophysical considerations. AAPG Bulletin. 1952; 36(2):278-98.
[29] Larionov WW. Borehole radiometry: Nedra. In: The SPWLA Annual Logging Symposium Transactions, 1969; 10, p. 26.
[30] Hilchie DW. Applied openhole log interpretation: Golden, Colorado, DW Hilchie. Inc., 161p. 1978; 1399:42-30.
[31] Ghorab, M., Mohmed A.M.R. and Nouh,, A.Z. The Relation Between the Shale Origin (Source or non Source) and its Type forAbu Roash Formation at Wadi El- Natrun Area, South of Western Desert, Egypt. Australian Journal of Basic and Appl Sci. 2008; 2(3):360-371.
[32] Keskes N, Boulanouar A, Lechevalier Y, Zaccagnino P. Image analysis techniques for seismic data. In *SEG Technical Program Expanded Abstracts 1982* (pp. 221-222). Society of Exploration Geophysicists.
[33] Faraklioti M, Petrou M. The use of structure tensors in the analysis of seismic data. Mathematical methods and modelling in hydrocarbon exploration and production. 2005:47-88.
[34] Avseth PA, Odegaard E. Well log and seismic data analysis using rock physics templates. First break. 2004; 22(10).
[35] Castagna JP. Petrophysical imaging using AVO. The Leading Edge. 1993; 12 (3):172-8.

[36] Chopra S, Marfurt KJ. Seismic attributes for prospect identification and reservoir characterization. Society of Exploration Geophysicists and European Association of Geoscientists and Engineers; 2007 Jan 1.
[37] Catuneanu O. Principles of sequence stratigraphy. Elsevier; 2006 May 19.
[38] Taner MT. Seismic attributes: Canadian Society of Exploration Geophysicists Recorder. 2001; pp 49–56.
[39] Naeem M, El-Araby HM, Khalil MK, Jafri MK, Khan F. Integrated study of seismic and well data for porosity estimation using multi-attribute transforms: a case study of Boonsville Field, Fort Worth Basin, Texas, USA. Arab J Geosci. 2015; 10:8777-8793. https://doi.org/10.1007/s12517-015-1806-7.
[40] Heinio P, Davies RJ. Knickpoint migration in submarine channels in response to fold growth, western Niger Delta. Marine and Petroleum Geology. 2007; 24(6-9): 434-449.

To whom correspondence should be addressed: Charles A. Illo, University of Nigeria, Nsukka, Department of Geology, Nigeria, E-mail: illocharles7@gmail.com